Multifluid Eulerian modeling of dense gas–solids fluidized bed hydrodynamics: Influence of the dissipation parameters

N. Reuge[a,*], L. Cadoret[a], C. Coufort-Saudejaud[a], S. Pannala[b], M. Syamlal[c], B. Caussat[a]

[a]Laboratoire de Génie Chimique, UMR CNRS 5503, ENSIACET/INPT, 5 rue Paulin Talabot, BP 1301, 31106 Toulouse Cedex 1, France
[b]Oak Ridge National Laboratory, Computer Science and Mathematics Division, Building 6012, MS-6367, RM-101, Oak Ridge, TN 37831, USA
[c]National Energy Technology Laboratory, 3610 Collins Ferry Road, P.O. Box 880, Morgantown, WV 26507-0880, USA

Keywords:
Fluidization
Powders
Mathematical modeling
Hydrodynamics
CFD
Validation

A B S T R A C T

Computational fluid dynamic (CFD) models must be thoroughly validated before they can be used with confidence for designing fluidized bed reactors. In this study, validation data were collected from a fluidized bed of (Geldart's group B) alumina particles operated at different gas velocities involving two fluidization hydrodynamic regimes (bubbling and slugging). The bed expansion, height of bed fluctuations and frequency of fluctuations were measured from videos of the fluidized bed. The Eulerian–Eulerian two fluid model MFIX was used to simulate the experiments. Two different models for the particle stresses—Schaeffer [Syamlal, M., Rogers, W., O'Brien, T.J., 1993. MFIX documentation: theory guide. Technical Report DOE/METC-94/1004 (DE9400087), Morgantown Energy Technology Centre, Morgantown, West Virginia (can be downloaded from Multiphase Flow with Interphase eXchanges (MFIX) website ⟨http://www.mfix.org⟩); Schaeffer, D.G., 1987. Instability in the evolution equations describing incompressible granular flow. Journal of Differential Equations 66, 61–74.] and Princeton [Srivastava, A., Sundaresan, S., 2003. Analysis of a frictional–kinetic model for gas–particle flow. Powder Technology 129(1–3), 72–85.] models—and different values of the restitution coefficient and internal angle of friction were evaluated. 3-D simulations are required for getting quantitative and qualitative agreement with experimental data. The results from the Princeton model are in better agreement with data than that from the Schaeffer model. Both free slip and Johnson–Jackson boundary conditions give nearly identical results. An increase in coefficient of restitution (e) from 0.8 to 1 leads to larger bed expansions and lower heights of fluctuations in the bubbling regime, whereas it leads to unchanged bed expansion and to a massive reduction in the height of fluctuations in the slugging regime. The angle of internal friction (ϕ) in the range 10–40° does not affect the bed expansion, but its reduction significantly reduces the height of fluctuations.

1. Introduction

Gas–solids fluidization is a technology presently used in chemical and biochemical processes such as drying, mixing and chemical reactions (Deen et al., 2007). The efficiency of such systems relies primarily on their hydrodynamic behavior. Therefore, the prediction of fluidized bed (FB) dynamics has been an active area of research for many years (Davidson and Harrison, 1963; Deen et al., 2006; Enwald et al., 1996). Thanks to the increase in the computational speed (Moore's law) and improved numerical algorithms, computational fluid dynamics (CFD) has become a promising tool for simulating FB dynamics.

Two phase flows can be modeled using two different approaches (Goldschmidt et al., 2001): the Lagrangian–Eulerian and the Eulerian–Eulerian models. Both consider the gas phase as a continuous phase. The fundamental difference between these two models lies in the way the particles are treated. The Lagrangian–Eulerian models describe the solids phase at the particle level, and the Newton's laws are applied to describe the motion of the particles. The Eulerian–Eulerian approach treats even the particles as a continuum, and the two phases form an interpenetrating continuum. As pointed out by Weber and Hrenya (2006), the Lagrangian models, being highly time consuming, are generally used in systems containing less than 100,000 particles in which some instantaneous interactions between particles (e.g., cohesion) must absolutely be taken into account. As a consequence, most of the recent works

* Corresponding author. Tel.: +33 5 34 61 52 52.
E-mail addresses: reuge@free.fr (N. Reuge), pannalas@ornl.gov (S. Pannala), Madhava.Syamlal@NETL.DOE.GOV (M. Syamlal), Brigitte.Caussat@ensiacet.fr (B. Caussat).

using the Lagrangian approach are devoted to the simulation of Geldart's group A and group C particles (Limtrakul et al., 2007; Tatemoto et al., 2005; Xu et al., 2002). For systems of larger size, the Eulerian–Eulerian models are usually preferred especially for the modeling of Geldart's group B powders (Lettieri et al., 2006; Patil et al., 2005; Taghipour et al., 2005).

Eulerian–Eulerian models require closure laws for particle interactions, and there is an absence of consensus concerning the stress terms in the particulate momentum equation. A typical FB includes dense regions where the particles are in enduring contacts (high solid volume fraction and the frictional or plastic stresses dominate), dilute regions where particles are in collisional contact (low solid volume fraction and the kinetic stresses dominate), and transition regions where the kinetic and the plastic stresses are equally important. The modeling of the kinetic stress based on the kinetic theory of granular flow (KTGF) is now generally accepted (Johansson et al., 2006; Lun et al., 1984; Taghipour et al., 2005; Van Wachem et al., 2001). By adopting theories mainly arising from the study of soil mechanics (e.g., Jackson, 1983; Massoudi, 1986; Schaeffer, 1987; Tuzun et al., 1982), several theories for describing the stresses in the plastic flow regime have been proposed. However, no theory exists for modeling transition regimes other than some way to combine kinetic theory with frictional theories. Thus, as pointed out by Srivastava and Sundaresan (2003), the "disparate nature of both contributions" leads to numerous questions about the way they should be combined. One of the first attempts was provided by Johnson and Jackson (1987) who proposed a model to describe shearing granular flows, combining both theories by simply adding the two formulas. Syamlal et al. (1993) proposed to consider the frictional stresses only at high solid volume fraction (i.e., for values higher than the solid fraction at minimum fluidization $\varepsilon_{s,mf}$) and used Schaeffer (1987) model for frictional stresses. This model is referred to in MFIX documentation as the Schaeffer model. In that model, the transition between the kinetic and the plastic regimes is thus rather abrupt and could lead, according to Makkawi et al. (2006), to inaccurate predictions of bubble shape and bed expansion in some specific cases (intermediate to high gas velocities). Another model proposed by Srivastava and Sundaresan (2003) is often called the Princeton model (Benyahia et al., 2006). Although the assumptions at the roots of this model are similar to those of Schaeffer (1987), the Princeton model also accounts for the strain rate fluctuations. In contrast to the model of Schaeffer (1987), frictional stresses in the model of Srivastava and Sundaresan (2003) influence the flow behavior even in the transition regions. They showed that the way the frictional stress is modeled considerably influences the shape of the bubble and also the bed dynamics.

In these closure laws, some physical parameters that characterize the particles are required, namely the coefficient of restitution (e) that reflects the energy dissipation due to particle–particle collisions and the internal angle of friction (ϕ) related to dissipation in the dense regime with enduring contacts. The significant sensitivity of both dense and dilute FB hydrodynamics to the value of e has been reported by numerous authors: experimentally by Chang and Louge (1992) and numerically by Chandrasekaran (2005), Goldschmidt et al. (2001), Hoomans et al. (1996), Lindborg et al. (2007), Pita and Sundaresan (1991) and Wang and Ge (2006). Goldschmidt et al. (2001) analyzed the influence of e by detailing all the terms of the pseudo-thermal energy equation (granular energy equation or conservation equation for the fluctuation energy of particles). They showed that the decrease of the restitution coefficient leads to a smaller number of elastic collisions resulting in an increase of the kinetic energy fluctuations generated by the particle pressure and the viscous shear, but that this energy is almost completely dissipated in inelastic collisions, resulting finally in a decrease of the granular temperature. These results have been confirmed by the recent work of Lindborg et al. (2007) and Wang and Ge (2006). As the restitution coefficient decreases, some regions of the bed become highly packed leading to sharper void fraction gradients and to large bubbles with a vigorous bubbling (Lu et al., 2005). Another direct consequence is that when more energy is dissipated, the gas pressure fluctuations across the bed increase. Using the commercial CFD code FLUENT, Taghipour et al. (2005) confirm that the hydrodynamic regime and bubble activity are closely linked to e, particularly for gas velocities beyond the minimum fluidization. They report that by decreasing the restitution coefficient, the bed expansion decreases. At last, they suggest that high values for e (e.g., 0.99) are required to simulate the dynamics of the FB for gas velocities above the minimum fluidization. It seems that the influence of ϕ on simulation results has been studied only by Chandrasekaran et al. (2005), who found that a decrease of the internal angle of friction resulted in smaller bubble sizes.

This paper reports a study about the influence of models for the solid phase stress and of the associated parameters on the dynamics of gas–solids FBs. Experimental measurements of the hydrodynamics of an FB composed of Geldart's group B alumina particles will be first presented. The numerical code and the two frictional stress models used (Schaeffer and Princeton), will be then described. The simulation results will be reported and compared with the experimental data, to highlight the influences of the use of 2-D or 3-D geometries, the frictional stress model, the coefficient of restitution, and the internal angle of friction.

2. Experimental investigations

2.1. Process description and operating conditions

Experiments were conducted in a cylindrical glass column of 1 m height and 5 cm internal diameter. Fluidization was performed with air at ambient temperature. The air flow rate was controlled by a ball flow meter (Brooks GT1355) associated with a manometer. At the bottom of the column, an inconel distributor of 40% of porosity provided a homogeneous gas distribution. A differential pressure gauge (Druck LPX5480) connected to an online monitoring system allowed measuring the pressure drop across the bed. A ruler has been placed along the glass column to determine the location of the bed surface.

Two alumina powders of different sizes were used. Their diameter distribution has been measured by a laser size analyzer (Mastersizer2000): the particle mean Sauter diameters (D_{32}) measured for the finest and for the coarsest powders were of 221 and 329 μm, respectively, and standard deviations of their volume size distributions were 58 and 77 μm, respectively. The alumina particles revealed to be non-porous, therefore their bulk density was equal to the density of alumina (i.e., 3900 kg/m^3). The two powders belonged clearly to the Geldart's group B and were easy to fluidize.

The mass of powders introduced in the column was fixed at 800 g, corresponding to a ratio of the bed height at packing to the column diameter of about 4. Several air flow rates were used in the range of 0.14–2.82 m^3/h STP, corresponding to superficial gas velocities U_g in the range of 0.02–0.4 m/s.

2.2. Experimental procedure

For all the processing conditions studied, the fluctuating bed was recorded using a tri-CCD camera (Panasonic NV-GS400) at a frame rate of 25 pictures per second. Then, consecutive frames of the videos corresponding to several cycles of bed fluctuations were analyzed. The bed surface was always well defined at the bed minimum, during the expansion, and at the bed maximum, allowing accurate

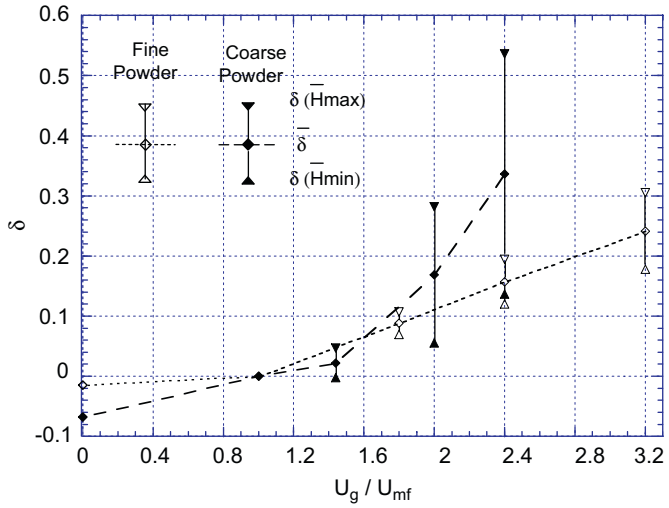

Fig. 1. Bed expansion ratio δ measured vs. relative gas velocity U_g/U_{mf} for fine and coarse powders.

measurements of the minimum and maximum bed heights. Note that the bed surface became diffuse only during the collapse because of the formation of a trail of few isolated particles falling down at a relatively slow speed. The analysis of 10 fluctuation cycles was sufficient to determine mean minimum and maximum bed heights $\overline{H}_{\min}$ and $\overline{H}_{\max}$ with an error margin of ±2%.

2.3. Experimental results

The minimum fluidization velocity (U_{mf}) of the fine powder was 0.05 m/s, corresponding to a bed height (H_{mf}) of 0.201 m and a void fraction (ε_{mf}) of 0.48. The plateau in the bed pressure drop was about 4000 Pa, very close to the theoretical value 3997 Pa. Decreasing the gas velocity to zero, the bed stabilized at a height of 0.198 m, which gives a void fraction at packing ε_0 of 0.472.

For the coarse powder, the measured minimum fluidization velocity (U_{mf}) was 0.125 m/s with a bed height (H_{mf}) of 0.227 m and a void fraction (ε_{mf}) of 0.54. The measured pressure drop was also very close to the theoretical value of 3997 Pa. At packing, the bed height was 0.212 m and ε_0 was 0.507.

Three superficial gas velocities U_g were specifically studied for the fine powder: 0.09, 0.12 and 0.16 m/s, corresponding to U_g/U_{mf} ratios of 1.8, 2.4 and 3.2, respectively. Three other gas velocities were investigated for the coarse powder: 0.18, 0.25 and 0.3 m/s, corresponding to U_g/U_{mf} ratios of 1.44, 2 and 2.4.

Measurements of bed heights as a function of gas velocity for the two powders are reported in Fig. 1 using the following expression for the ratio of bed expansion:

$$\delta(H) = \frac{H - H_{mf}}{H_{mf}}. \tag{1}$$

We define the mean bed expansion ratio by

$$\overline{\delta} = \delta\left(\frac{\overline{H}_{\max} + \overline{H}_{\min}}{2}\right) \tag{2}$$

and the relative height of fluctuations by

$$\Delta\delta = \delta(\overline{H}_{\max}) - \delta(\overline{H}_{\min}), \tag{3}$$

where $\overline{H}$ is the mean expanded bed height.

For the two powders, as can be seen in Fig. 1, $\overline{\delta}$ and $\Delta\delta$ increase with gas velocity. For U_g/U_{mf} equal to 2.4, values of $\overline{\delta}$ and $\Delta\delta$ measured for the fine powder are of 15.7% and 7.5%, respectively, whereas for the coarse powder, they are of 33% and 40%, respectively. It can be also deduced from these measurements that, for a given expansion ratio, the bed of coarse powder undergoes larger fluctuations than the bed of fine powder (about 2 times).

These results can be explained by the observation from the videos that the bed of fine powder remained in the bubbling regime for all the conditions tested, whereas the bed of coarse powder passed from the bubbling regime to the slugging regime at a value of U_g/U_{mf} around 2 (i.e., $U_g = 0.25$ m/s).

3. Numerical model

Open source simulation software MFIX (http://www.mfix.org) has been used for this study. As mentioned before, the interpenetrating continuum model is used to simulate the current gas–solid system with one phase representing the gas and the other phase representing the solid. The summary of the governing equations and the granular stress models employed are given below and the details can be obtained from MFIX documentation (Benyahia et al., 2006; Syamlal et al., 1993). The numerical method employed for time discretization is implicit backward Euler method and for the convective terms discretization is superbee or first-order upwind. The set of non-linear equations is linearized using a modified version of the SIMPLE (Patankar, 1980) algorithm using void fraction and gas pressure correction equations. The resulting system of sparse, non-symmetric linear equations for each of the equations is solved using BiCGStab method (Barrett et al., 2006) algorithm. More details are available in the MFIX numerical guide (Syamlal, 1998).

3.1. Governing equations

The governing equations solved for the current gas–solid system are:

Continuity for phase k ($k = g$ for gas or m for solids):

$$\frac{\partial}{\partial t}(\varepsilon_k \rho_k) + \frac{\partial}{\partial x_i}(\varepsilon_k \rho_k u_{ki}) = 0. \tag{4}$$

Momentum conservation for phase k:

$$\left[\frac{\partial}{\partial t}(\varepsilon_k \rho_k u_{ki}) + \frac{\partial}{\partial x_j}(\varepsilon_k \rho_k u_{kj} u_{ki})\right] = -\varepsilon_k \frac{\partial P_g}{\partial x_i} + \frac{\partial \tau_{kij}}{\partial x_j} + \sum_{\substack{k'=g,m \\ k' \neq k}} I_{k'ki} + \varepsilon_k \rho_k g_i + \delta_{kg} f_{gi}. \tag{5}$$

Here, ε stands for volume fraction, ρ stands for density, u for velocity, P for pressure and g for gravitational acceleration. Beyond the single-phase Navier–Stokes equation, the momentum equation (5) for solid phase m has two additional terms that need to be closed. The first term is the interfacial drag term (I_{gmi}) and the second one is for the solid phase stresses (τ_{mij}). The drag formula used in this paper is that postulated by Syamlal and O'Brien (2003) (Benyahia et al., 2006). It is given by product of the drag interaction term and relative velocity:

$$I_{gmi} = \beta_{gm}(u_{gi} - u_{mi}), \tag{6}$$

where the drag interaction term is defined as

$$\beta_{gm} = \frac{3\varepsilon_m \varepsilon_g \rho_g}{4 V_{rm}^2 d_p}(0.63 + 4.8\sqrt{V_{rm}/Re_m})^2 |\mathbf{u}_g - \mathbf{u}_m|, \tag{7}$$

where d_p stands for the particle diameter, Re stands for the particle Reynolds number ($Re_m = d_p|\mathbf{u}_g - \mathbf{u}_m|\rho_g/\mu_g$) and the non-dimensional

parameter V_{rm} is given as

$$V_{rm} = 0.5(A - 0.06Re_m + \sqrt{(0.06Re_m)^2 + 0.12Re_m(2B - A) + A^2}), \tag{8}$$

where A and B are given as

$$A = \varepsilon_g^{4.14}, \tag{9}$$

$$B = \begin{cases} c\varepsilon_g^{1.28} & \text{if } \varepsilon_g \leqslant 0.85, \\ \varepsilon_g^{d} & \text{if } \varepsilon_g > 0.85. \end{cases} \tag{10}$$

The drag constants c and d were determined from the physical properties of the carrier gas, powder properties (density, Sauter diameter), experimentally measured minimum fluidization velocity (U_{mf}), and the mean void fraction at U_{mf} (Syamlal and O'Brien, 2003). Once c and d are fixed, they are not varied for changes in operating parameters like gas velocity.

3.2. Granular stress models

The solid stresses in Eq. (5) are given by

$$\tau_{mij} = \left(-P_m + \eta\mu_b \frac{\partial u_{mi}}{\partial x_i}\right)\delta_{ij} + 2\mu_m S_{mij}, \tag{11}$$

where

$$S_{mij} = \frac{1}{2}\left(\frac{\partial u_{mi}}{\partial x_j} + \frac{\partial u_{mj}}{\partial x_i}\right) - \frac{1}{3}\frac{\partial u_{mi}}{\partial x_j}, \tag{12}$$

the solids pressure,

$$P_m = \varepsilon_m \rho_m \Theta_m [1 + 4\eta\varepsilon_m g_0] \tag{13}$$

and solids viscosity,

$$\mu_m = \left(\frac{2+\alpha}{3}\right)\left[\frac{\mu_m^*}{g_0\eta(2-\eta)}\left(1 + \frac{8}{5}\eta\varepsilon_m g_0\right) \times \left(1 + \frac{8}{5}\eta(3\eta - 2)\varepsilon_m g_0\right) + \frac{3}{5}\eta\mu_b\right], \tag{14}$$

where

$$\mu_m^* = \frac{\rho_m \varepsilon_m g_0 \Theta_m \mu'}{\rho_m \varepsilon_m g_0 \Theta_m + (2\beta\mu'/\rho_m\varepsilon_m)}, \tag{15}$$

$$\mu' = \frac{5}{96}\rho_m d_p \sqrt{\pi\Theta_m} \tag{16}$$

and

$$\mu_b = \frac{256}{5\pi}\mu'\varepsilon_m^2 g_0. \tag{17}$$

Here, g_0 is the radial function and Θ is the granular temperature. Granular energy transport equation of the following form is used to solve for Θ:

$$\frac{3}{2}\varepsilon_m\rho_m\left[\frac{\partial\Theta_m}{\partial t} + u_{mj}\frac{\partial\Theta_m}{\partial x_j}\right] = \frac{\partial}{\partial x_i}\left(\kappa_m\frac{\partial\Theta_m}{\partial x_i}\right) + \tau_{mij}\frac{\partial u_{mi}}{\partial x_j} + \Pi_m - \varepsilon_m\rho_m J_m, \tag{18}$$

where the solid conductivity of granular energy κ_m is given by

$$\kappa_m = \left(\frac{\kappa_m^*}{g_0}\right)\left[\left(1 + \frac{12}{5}\eta\varepsilon_m g_0\right)\left(1 + \frac{12}{5}\eta^2(4\eta - 3)\varepsilon_m g_0\right) + \frac{64}{25\pi}(41 - 33\eta)\eta^2(\varepsilon_m g_0)^2\right], \tag{19}$$

where

$$\kappa_m^* = \frac{\rho_m\varepsilon_m g_0\Theta_m\kappa}{\rho_m\varepsilon_m g_0\Theta_m + \left(\frac{6\beta_{gm}\kappa}{5\rho_m\varepsilon_m}\right)} \tag{20}$$

and

$$\kappa = \frac{75\rho_m d_p\sqrt{\pi\Theta_m}}{48\eta(41 - 33\eta)}, \tag{21}$$

collisional dissipation is given by

$$J_m = \frac{48}{\sqrt{\pi}}\eta(1-\eta)\frac{\varepsilon_m g_0}{d_p}\Theta_m^{3/2}, \tag{22}$$

$$\eta = \frac{1+e}{2}, \tag{23}$$

and exchange terms are given by

$$\Pi_m = -3\beta_{gm}\Theta_m + \frac{81\varepsilon_m\mu_g^2|\mathbf{u}_g - \mathbf{u}_m|^2}{g_0 d_p^3\rho_m\sqrt{\pi\Theta_m}}. \tag{24}$$

The above model is used in the dilute regime of the particle flow while the following two options are exercised as the particles approach the packing limit and frictional stresses are generated.

3.2.1. Schaeffer model

In this model (Schaeffer, 1987; Syamlal et al., 1993), at the critical state when the solid volume fraction exceeds the maximum packing limit, the following relations are used to calculate the solid pressure and viscosity:

$$P_c = \begin{cases} 10^{25}(\varepsilon_g^* - \varepsilon_g)^{10}, & \varepsilon_g < \varepsilon_g^*, \\ 0, & \varepsilon_g \geqslant \varepsilon_g^*, \end{cases} \tag{25}$$

$$\mu_f = \begin{cases} \min\left(\frac{P_c\sin(\phi)}{\sqrt{4I_{2D}}}, \mu_m^{\max}\right), & \varepsilon_g < \varepsilon_g^*, \\ 0, & \varepsilon_g \geqslant \varepsilon_g^*, \end{cases} \tag{26}$$

where $\mu_m^{\max} = 1000\,\mathrm{P}$,

$$I_{2D} = \frac{1}{6}[(D_{m,11} - D_{m,22})^2 + (D_{m,22} - D_{m,33})^2 + (D_{m,33} - D_{m,11})^2] + D_{m,12}^2 + D_{m,23}^2 + D_{m,31}^2 \tag{27}$$

and

$$D_{m,ij} = \frac{1}{2}\left(\frac{\partial u_{m,i}}{\partial x_j} + \frac{\partial u_{m,j}}{\partial x_i}\right). \tag{28}$$

With this model, we have assumed (as typically approximated) that the critical void fraction ε_g^* below which pure frictional stress occurs is equal to ε_{mf}.

3.2.2. Princeton model

This model (Srivastava and Sundaresan, 2003) is a modification of the Savage (1998) model that accounts for strain rate fluctuations. This frictional stress model influences the flow behavior at solid volume fractions below maximum packing:

$$P_c = \begin{cases} 10^{25}(\varepsilon_g^* - \varepsilon_g)^{10}, & \varepsilon_g < \varepsilon_g^*, \\ \mathrm{Fr}\,\frac{((1-\varepsilon_g) - \varepsilon_{sf}^{\min})^r}{(\varepsilon_g - \varepsilon_g^*)^s}, & \varepsilon_g^* \leqslant \varepsilon_g < (1 - \varepsilon_{sf}^{\min}), \\ 0, & \varepsilon_g \geqslant (1 - \varepsilon_{sf}^{\min}), \end{cases} \tag{29}$$

where $\mathrm{Fr} = 0.5$, $r = 2$, $s = 5$.

The solid pressure is given as

$$\frac{P_f}{P_c} = \left(1 - \frac{\nabla \cdot \mathbf{u}_m}{n\sqrt{2}\sin(\varphi)\sqrt{\mathbf{S}:\mathbf{S} + \Theta_m/d_p^2}}\right)^{n-1}, \tag{30}$$

and the viscosity is

$$\mu_f = \frac{\sqrt{2}P_f \sin(\varphi)}{\sqrt{\mathbf{S}:\mathbf{S} + \Theta_m/d_p^2}} \left\{ n - (n-1)\left(\frac{P_f}{P_c}\right)^{1/(n-1)} \right\}. \tag{31}$$

Here, the coefficient n is set differently depending on whether the granular assembly is undergoing a dilatation or compaction:

$$n = \begin{cases} \dfrac{\sqrt{3}}{2\sin(\phi)}, & \nabla \cdot \mathbf{u}_m \geqslant 0, \\ 1.03, & \nabla \cdot \mathbf{u}_m < 0 \end{cases} \tag{32}$$

and the bulk viscosity is set by the following relation:

$$\mu_f^{\text{bulk}} = -\frac{2}{3}\mu_f. \tag{33}$$

With the Princeton model, it is typical to assume that the critical void fraction (ε_g^*) below which pure frictional stress occurs is equal to the void fraction at packing (ε_0) and that the high limit void fraction above which frictional stresses no longer play a role (i.e., $1 - \varepsilon_{sf}^{\min}$) equals ε_{mf}.

3.3. Johnson and Jackson wall boundary conditions

Johnson and Jackson (1987) boundary conditions account for partial slip of the solids at the walls. Tangential solids velocity and the granular energy at the walls are given by

$$\mu_m \frac{\partial u_m}{\partial x} = -\frac{\phi_p \pi \rho_m \varepsilon_m g_0 \sqrt{\Theta_m}}{2\sqrt{3}\varepsilon_m^{\max}} u_m, \tag{34}$$

$$\kappa_m \frac{\partial \Theta_m}{\partial x} = \frac{\phi_p \pi u_m^2 \rho_m \varepsilon_m g_0 \sqrt{\Theta_m}}{2\sqrt{3}\varepsilon_m^{\max}} - \frac{\sqrt{3}\pi \rho_m \varepsilon_m g_0 (1 - e_w^2)\sqrt{\Theta_m}}{4\varepsilon_m^{\max}} \Theta_m. \tag{35}$$

4. Simulation

4.1. Input parameters and data processing

All the experimental parameters used for the simulations are given in Table 1. Using the Schaeffer (1987) model (Syamlal et al., 1993) and the Princeton model (Srivastava and Sundaresan, 2003) to calculate solid stresses in the frictional regime, 2-D axisymmetric, 2-D Cartesian and 3-D MFIX simulations were performed for the three gas velocities studied as detailed in Section 4.3.1. The coefficients of the Syamlal–O'Brien (2003) drag correlation c and d were determined from the physical properties of the carrier gas, powder properties, experimentally measured minimum fluidization velocity (U_{mf}), and the mean void fraction at U_{mf}. Their values for the two powders are given in Table 1. Since we did not find any data in the literature for the restitution coefficient for the collisions of alumina particles, the default value of 0.8 was used, and then higher values were tested as explained in Section 4.3.2. In all the simulations, the coefficient of restitution for particle–wall collisions (e_w) was set to 1. The internal angle of friction was first fixed to 40°, which is the experimentally determined angle of repose of the two powders. Indeed, for non-cohesive powders, these two parameters are identical (Terzaghi, 1942). Then, values of 30° and 10° were tested and the effects on the results are discussed in Section 4.3.3. Regarding wall boundary conditions (BCs), no slip for gas and Johnson and Jackson (J & J) partial slip for solids were used. Also free slip for solids was tested, as discussed below.

Particular care was taken for the analysis of the simulation results. First, a void fraction of 0.95 was shown to define the bed surface with reasonable accuracy. Taking a value of 0.9 or 0.99 did not change the results very significantly (this point will be discussed later) at the bed minimum, during the expansion stage and at the bed maximum, meaning that the bed surface was well defined just as in the experiments (formation of a trail observed during the collapse was also reproduced by the calculations). Then, the void fraction values near the wall (for comparison with experimental data) were extracted and averaged in the azimuthal direction. From the axial profile of the void fraction, the height of the bed surface was determined for every 0.01 s. A moving-average filter (with a width of 2-time steps) was then applied to these temporal evolutions of bed heights to remove point-to-point fluctuations. A routine was used to extract minimum and maximum bed heights and their temporal positions. Since small secondary peaks appeared randomly along the main fluctuations, specific tests had to be implemented in this routine to determine the true minima and maxima. Average bed heights $\overline{H}_{\min}$ and $\overline{H}_{\max}$ were finally determined from a minimum of 10 fluctuations (typically 6 s) similar to the analysis of the experimental data. The initial transient fluctuations were ignored for the data analysis because the bed hydrodynamics is dependent on the initial conditions for the first few seconds (from 1 to 3 s depending on U_g).

4.2. Discretization scheme and grid refinement

A preliminary study was initially conducted to aid the choice of the suitable discretization schemes as well as grid resolution for the current validation exercise. Both first- and second-order schemes for different grid resolutions were employed and their influence on bed height and magnitudes of fluctuations were used as the criteria for selecting the optimal scheme and grid resolution.

These simulations were performed with a consistent set of parameters for two extreme operating conditions: fine powder—U_g/U_{mf} = 1.8/coarse powder—U_g/U_{mf} = 2.4. For both these operating conditions, very similar effects of the discretization scheme and the grid resolution on bed expansion and height of fluctuation were found. The results for the operating condition "coarse powder—U_g/U_{mf} = 2.4" are presented in Fig. 2: irrespective of the discretization scheme, the grid resolution of 15 × 300 × 6 (i.e., 27,000 cells, 15 cells along the radial direction for the half diameter, 300 cells along the axial

Table 1
Experimental and simulation parameters

	ρ (kg/m^3)	D_{32} (μm)	m_p (kg)	H_0–ε_0 (m, dimensionless)	U_{mf}–H_{mf}–ε_{mf} (m/s, m, dimensionless)	U_g tested (m/s)	$c - d$ (dimensionless)	$e - \phi$ tested (dimensionless-deg)
Fine powder	3900	221	0.8	0.198–0.472	0.05–0.201–0.48	0.09–0.12–0.16	0.137–13.51	0.8–10°, 0.8–30°, 0.8–40°
Coarse powder	3900	329	0.8	0.212–0.507	0.125–0.227–0.54	0.18–0.25–0.30	0.165–12.38	0.9–40°, 0.99–40°, 1–40°

direction for a height of 0.6 m—or in other words almost square cells of about 2 mm, around 10 times the particles diameters—and six cells in the circumferential direction) seemed sufficient to obtain bed expansion and height of fluctuation that are independent of the grid resolution. The use of very coarse grids leads to underestimation of heights of fluctuation and typically, simulations performed with the second-order discretization scheme for a given grid resolution leads to more accurate results and for a given accuracy leads to 100 times shorter computational times compared with simulations performed with the first-order upwind discretization scheme.

Therefore, we choose the second-order scheme and the grid resolution of $15 \times 300(\times 6)$ for the subsequent 2-D and 3-D simulations. The grid size of the order of a few particle diameters used in this study is usually adequate for resolving the meso-scale structures of gas–solid flows (Agrawal et al., 2001).

4.3. Results and comparisons

4.3.1. 2-D/3-D simulations and Schaeffer/Princeton solid stress models

All calculations presented in this section were performed with e of 0.8 and ϕ of 40°. Unless otherwise specified, the wall BC used for solids is Johnson and Jackson partial slip BC and no slip for gas. Expansion ratios ($\overline{\delta}$) and relative heights of fluctuation calculated for the fine powder are reported in Figs. 3a and b, respectively. The same quantities calculated for the coarse powder are reported in Figs. 4a and b, respectively. Irrespective of the powder and the solid stress model used, it appears that all calculations overestimate $\overline{\delta}$ and $\Delta\delta$. But the 3-D simulation results are much closer to experimental data than the 2-D simulation results. For instance, at the highest gas velocity for the fine powder, the $\overline{\delta}$ and $\Delta\delta$ calculated with the Schaeffer model are around 2.2 and 2.7 times larger than the respective experimental values in the 2-D axisymmetric simulation, whereas they are only around 1.1 and 1.3 times larger than the respective experimental values in the 3-D simulation. 2-D axisymmetric calculations using the Princeton model give better results than those performed with the Schaeffer model but discrepancies are still very large. 2-D Cartesian calculations (performed with the Princeton model) are closer to experiments and the 3-D calculations than 2-D axisymmetric calculations, but still overestimate significantly the bed expansions and heights of fluctuation.

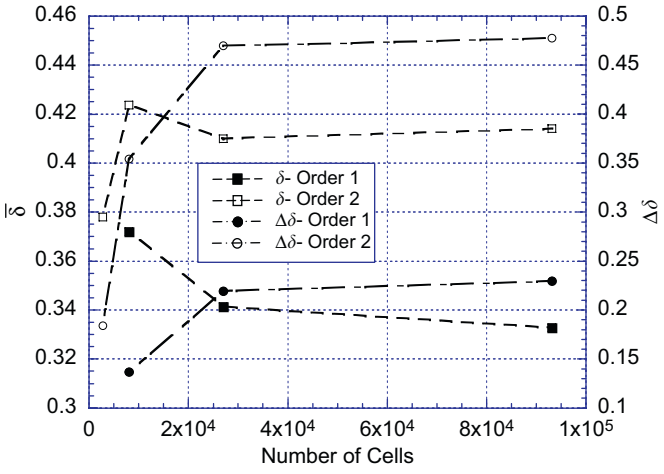

Fig. 2. Effect of discretization schemes and grid resolution on expansion ratio and relative fluctuation—coarse powder, $U_g/U_{mf}=2.4$—grids used: $7\times133\times3$, $10\times200\times4$, $15\times300\times6$, $23\times450\times9$.

In terms of bed expansion, 3-D calculations give almost identical results for both the frictional stress models (see Figs. 3a and 4a) and reproduce very well the experiments for the fine powder (see Fig. 3a). In terms of bed fluctuations, 3-D calculations using the Princeton model yield always significantly better results than 3-D calculations using the Schaeffer model (see Figs. 3b and 4b). The experimental bed expansion curve for coarse powder (Fig. 4a) is qualitatively different from that for the fine powder (Fig. 3a), whereas the simulated bed expansion curves look similar. Overall, 3-D calculations with the Princeton model give consistently better results.

Another difference between 2-D axisymmetric and 3-D calculations is that they predict significantly different radial profiles of void fraction as shown in Fig. 5. In this figure, the void fractions presented correspond to radial profiles of void fraction averaged over the axial direction between 0.1 and 0.2 m, over the azimuthal direction, and over 6 s of time. 3-D calculations result in void fractions steadily increasing, except near the walls, from the column wall to the column center, whereas 2-D calculations lead to a maximum in void fraction at half-radius of the column and overestimate the solid fractions at the column center. This 2-D effect is always present, but the magnitude of the effect depends on the gas velocity and the axial position in the column. This has been also illustrated in Cadoret et al. (2007) and had been highlighted previously by Guenther et al. (2001) and Xie et al. (2008a,b). This is due to the numerical artifact that the solids cannot cross the centerline boundary and are artificially reflected from this boundary.

This numerical artifact also explains why 2-D axisymmetric calculations overpredict bed expansion and heights of fluctuation. The 2-D Cartesian calculations differ because the third direction for relaxation is absent and some of the additional terms in the circumferential direction start playing a role in the dynamics (Xie et al., 2008a,b).

Moreover, in the 3-D calculations the Princeton model predicts a small decrease in the void fraction near the wall compared with the

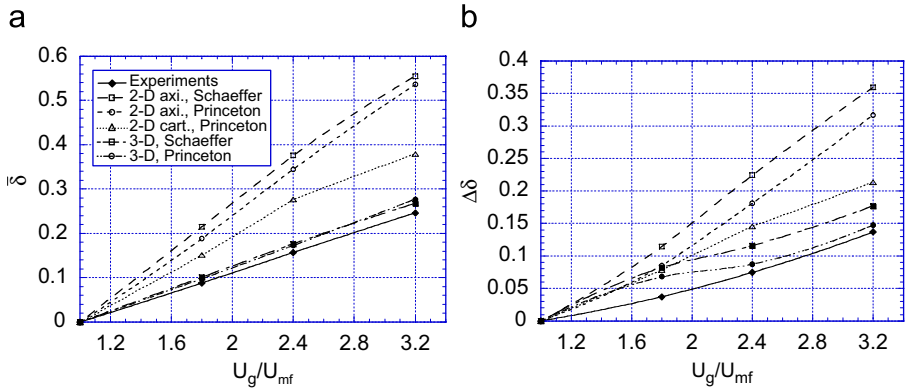

Fig. 3. (a) Bed expansion ratio δ calculated vs. relative gas velocity U_g/U_{mf}, 2-D/3-D calculations, Schaeffer/Princeton solid stress models, fine powder. (b) Relative height of fluctuation $\Delta\delta$ calculated vs. relative gas velocity U_g/U_{mf}, 2-D/3-D calculations, Schaeffer/Princeton solid stress model, fine powder.

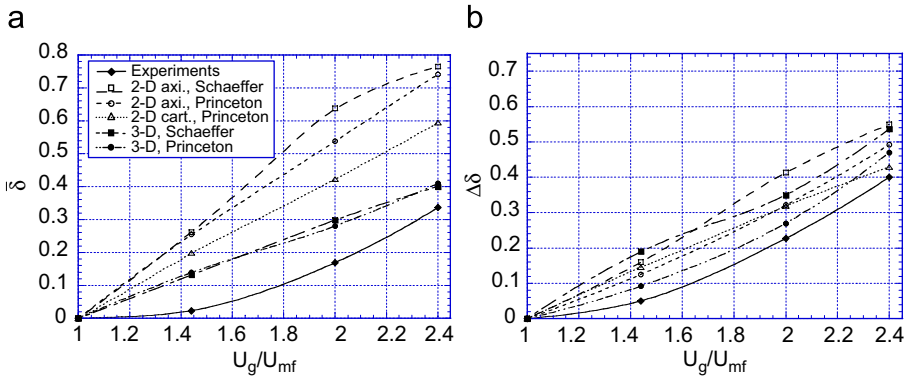

Fig. 4. (a) Bed expansion ratio δ calculated vs. relative gas velocity U_g/U_{mf}, 2-D/3-D calculations, Schaeffer/Princeton solid stress model, coarse powder. (b) Relative height of fluctuation $\Delta\delta$ calculated vs. relative gas velocity U_g/U_{mf}, 2-D/3-D calculations, Schaeffer/Princeton solid stress model, coarse powder.

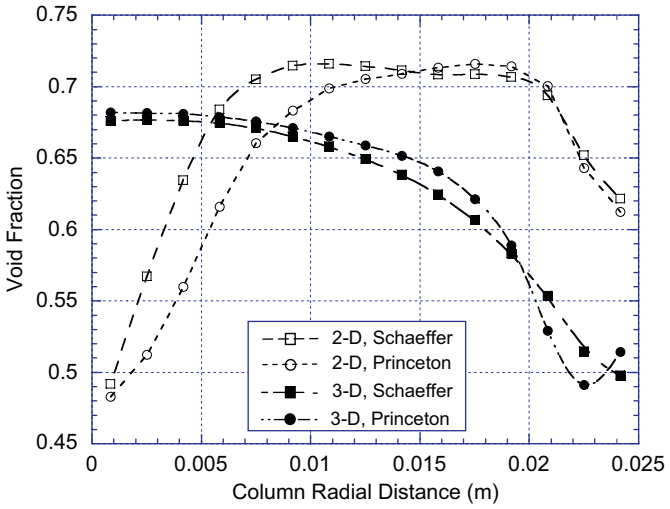

Fig. 5. Radial profiles of void fraction temporally averaged over 6 s and spatially averaged over column height from 10 to 20 cm, 2-D/3-D calculations, Schaeffer/Princeton solid stress model, fine powder, $U_g/U_{mf} = 3.2$.

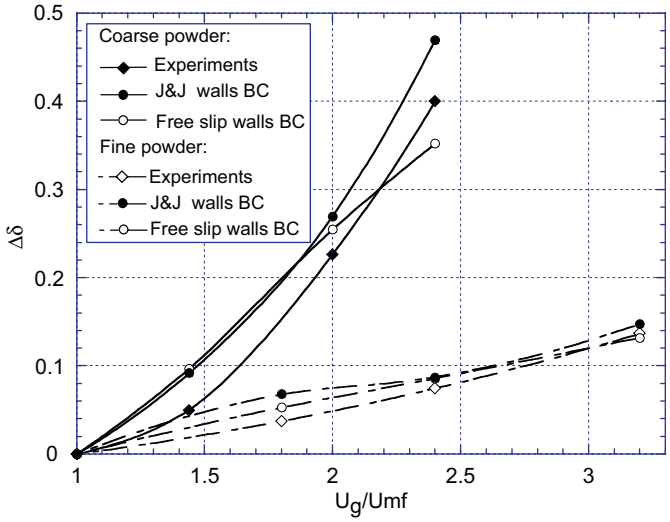

Fig. 6. Relative height of fluctuation $\Delta\delta$ calculated vs. relative gas velocity U_g/U_{mf}, free sleep/Johnson and Jackson wall BC for solids, fine and coarse powders.

Schaeffer model. Note that the 3-D representation was used for all the following simulations.

Note that instead of J&J partial slip BC, free slip BC was tested for solids with the Princeton model for both powders. The bed expansions calculated were nearly identical, whereas the free slip wall BC tends to decrease the fluctuations as shown in Fig. 6. Nevertheless, the difference becomes really important only for the coarse powder with $U_g/U_{mf} = 2.4$ (i.e., in a strong slugging regime) since the value of $\Delta\delta$ is 33% greater with J&J partial slip as compared to the free slip wall BC. However, from this study it cannot be concluded which of these two wall BCs are a better representation of the experiments; it can be just deduced that free slip wall BC tends to underestimate the heights of fluctuations at high gas velocities, whereas J&J wall BC tends to overestimate them.

For the fine powder with $U_g/U_{mf} = 3.2$ and for the coarse powder with $U_g/U_{mf} = 2.4$, Figs. 7a and b show photographs extracted from the experimental videos and instantaneous void fractions extracted from the calculations with the Princeton model. Photographs of the real bed are views through the wall while the simulation fields are slices through the bed axis. They have been chosen such that the beds are at their maximum expansion state. One can see that sizes and typical forms of bubbles calculated are qualitatively in good agreement with the experiments. In addition, one can compare the forms of bubbles and slugs obtained with J&J wall BC (Fig. 7b1) and free slip wall BC for solids (Fig. 7b2): an annular secondary bubble in contact with the walls and surrounding the lower part of the main slug is seen with J&J BC. This phenomenon is clearly perceptible only for the coarse powder at high velocities but also occurs for the fine powders as indicated in Fig. 5.

Moreover, these views show that bed surfaces are very well defined. This visual impression is confirmed by data processing since taking 0.99 instead of 0.95 as a value of void fraction for defining the bed surface, bed heights would increase only by 2% in average and the amplitude of fluctuations would decrease by 3%.

For the fine powder with $U_g/U_{mf} = 3.2$ and for the coarse powder with $U_g/U_{mf} = 2.4$, Figs. 8a and b show the temporal evolutions of measured and calculated bed heights. Both simulations have been performed using the Princeton model and J&J BC. Concerning the calculated bed heights, as previously mentioned, small secondary peaks sometimes appear (see for example around 3.8 s in Fig. 8a): these peaks result from parts of the main bubbles that are not completely coalesced. As mentioned before, the data processing ignored these small secondary peaks and considered only true minima and maxima. The same procedure was applied to extract manually true minima and maxima from the experimental videos. The important point is that the same consistent criteria for detecting minima and maxima (such as a minimum periodicity between two minima and/or maxima) were applied for processing experimental and simulation

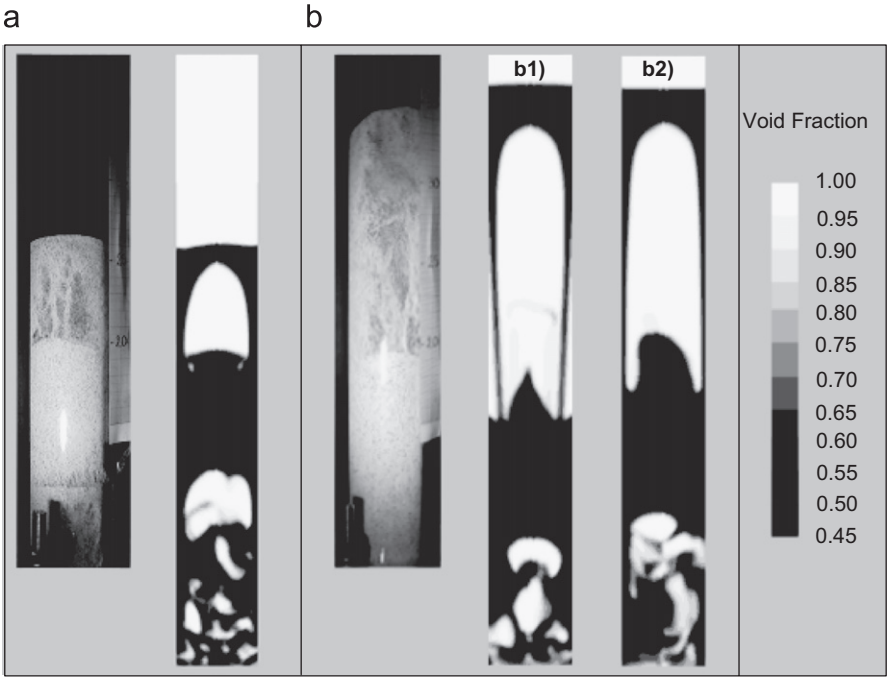

Fig. 7. Comparisons between photographs of the bed and instantaneous void fractions calculated with the Princeton model for (a) fine powder, $U_g/U_{mf} = 3.2$, $t = 2.68$ s, (b1) coarse powder, $U_g/U_{mf} = 2.4$, $t = 2.37$ s, J&J wall BC and (b2) $t = 3.55$ s, free sleep wall BC for solids.

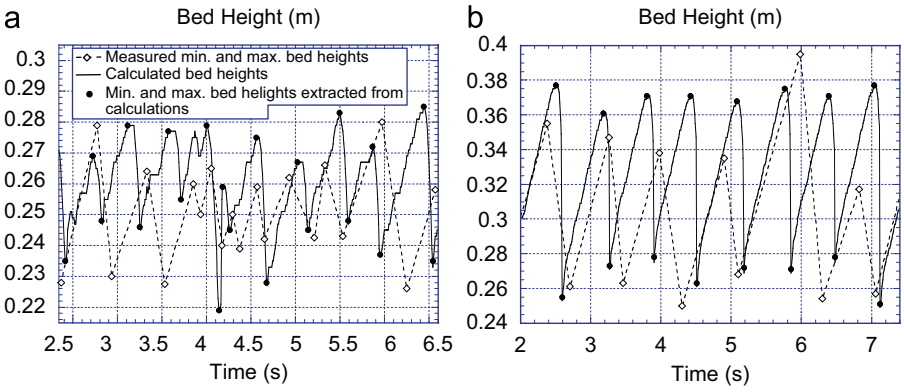

Fig. 8. Temporal evolutions of measured and calculated bed heights for (a) fine powder, $U_g/U_{mf} = 3.2$ and (b) coarse powder, $U_g/U_{mf} = 2.4$.

data. The similarity of these experimental and calculated transient curves confirms that the model predicts the bed dynamics for the cases tested with reasonable accuracy.

Except for the coarse powder at a U_g/U_{mf} ratio of 1.44, all fluctuation frequencies are overpredicted by 3-D simulations as shown by Fig. 9. With the Princeton model, the overestimations are roughly of 0.4 fluctuations per second. With the Schaeffer model, results are better, particularly for the fine powder. Nevertheless, discrepancies stay moderate, even with the Princeton model.

Overall, it can be concluded that the bed expansion ratio, the height of fluctuations, and the fluctuation frequencies can be satisfactorily reproduced using the Princeton model implemented in MFIX.

4.3.2. Influence of the restitution coefficient

Let us recall that the real value of e for our alumina particles being unknown, the default value of 0.8 was used for the previous calculations. Actually, the restitution coefficient varies with both properties of the colliding particles (material, surface shape, roughness, etc.) and their relative velocities (Ding et al., 2001; Gorham and Kharaz, 2000; Helland et al., 2005). In practice, using a value of 0.8 is often a reasonable choice. But alumina being a very hard material undergoing minimal plastic strain, a higher value could be presumed. This led us to redo all 3-D calculations with the value of 1 for pure elastic collisions.

For the fine powder, increasing the value of e from 0.8 to 1 leads to greater bed expansions, as reported in Fig. 10a. It is particularly true with the Princeton model, which predicts $\overline{\delta}$ correctly using a value of e of 0.8 but overestimates $\overline{\delta}$ by a factor around 1.4 when the value of e is 1. As shown in Fig. 10b, the other effect is to decrease the heights of fluctuation. This is very significant with the Princeton model at $U_g/U_{mf} = 3.2$ because increasing the value of e from 0.8 to 1 reduces $\Delta\delta$ by a factor of 3. Another consequence is that heights of fluctuation calculated with the Schaeffer model becomes closer to experiment when e is increased to 1.

However, for the coarse powder when e is increased to 1, no significant increase of bed expansion is obtained with the

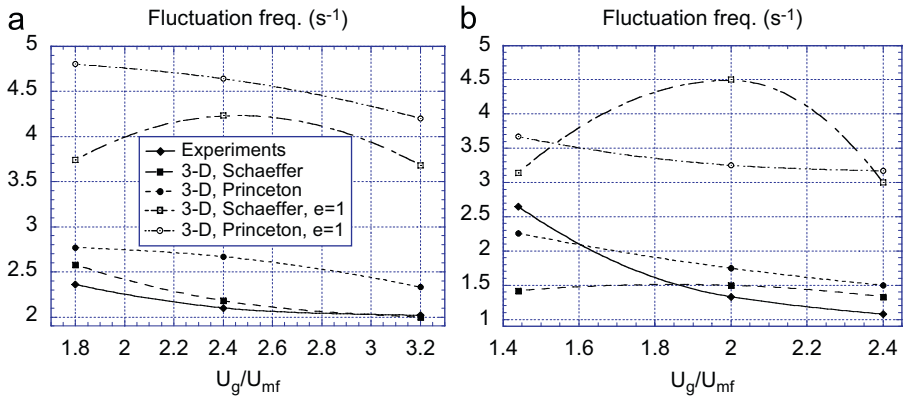

Fig. 9. (a) Fluctuation frequency calculated vs. relative gas velocity U_g/U_{mf}, 3-D calculations, Schaeffer/Princeton solid stress models, restitution coefficient of 0.8/1, fine powder. (b) Fluctuation frequency calculated vs. relative gas velocity U_g/U_{mf}, 3-D calculations, Schaeffer/Princeton solid stress model, restitution coefficient of 0.8/1, coarse powder.

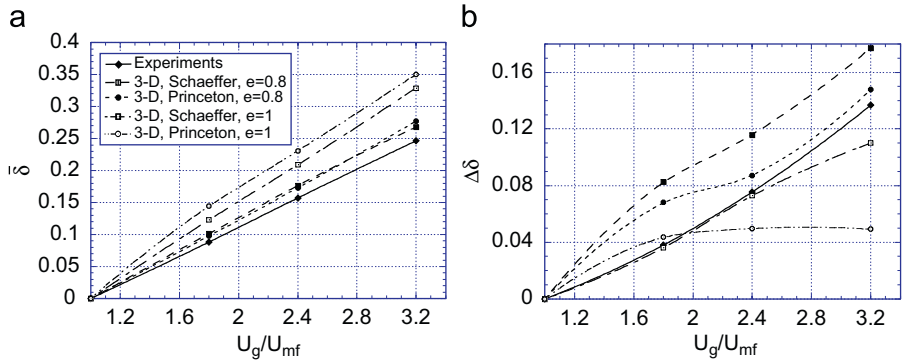

Fig. 10. (a) Bed expansion ratio δ calculated vs. relative gas velocity U_g/U_{mf}, 3-D calculations, Schaeffer/Princeton solid stress model, restitution coefficient of 0.8/1, fine powder. (b) Relative height of fluctuation $\Delta\delta$ calculated vs. relative gas velocity U_g/U_{mf}, 3-D calculations, Schaeffer/Princeton solid stress model, restitution coefficient of 0.8/1, fine powder.

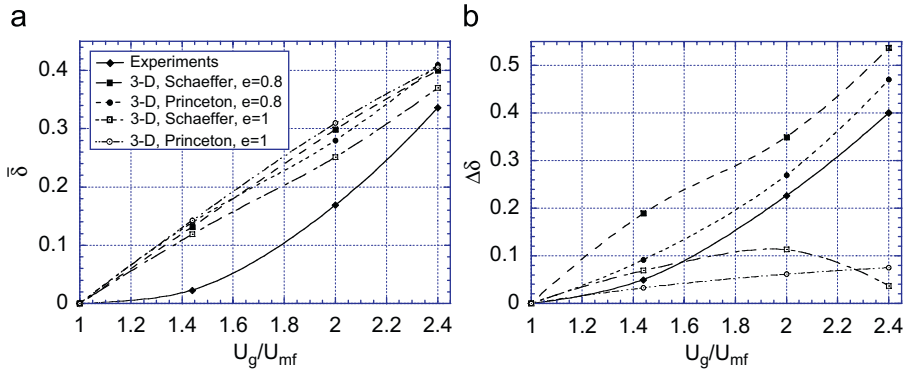

Fig. 11. (a) Bed expansion ratio δ calculated vs. relative gas velocity U_g/U_{mf}, 3-D calculations, Schaeffer/Princeton solid stress model, restitution coefficient of 0.8/1, fine powder. (b) Relative height of fluctuation $\Delta\delta$ calculated vs. relative gas velocity U_g/U_{mf}, 3-D calculations, Schaeffer/Princeton solid stress model, restitution coefficient of 0.8/1, coarse powder.

Princeton model (see Fig. 11a). But the Schaeffer model predicts decreased bed expansion, in contrast to the behavior obtained with the fine powder. This means that in the bubbling regime, an increase of e induces higher bed expansions, whereas in the slugging regime, the effect becomes insignificant or opposite. There is no simple physical explanation for these results as these dynamics seem to evolve from a complex interaction between the energy dissipated in the dilute kinetic regions of the bed and in the dense frictional regions of the bed.

The heights of fluctuations still decrease when e is increased to 1 (Fig. 11b). At high velocities ($U_g/U_{mf} = 2.4$), the value of $\Delta\delta$ dramatically decreases to about 10% of its value at $e = 0.8$ (which is close to experimental data).

Additional simulations were also performed with particle–particle restitution coefficient of 0.9 and 0.99 for the coarse powder with the Princeton model. The noteworthy results are presented in Fig. 12 showing a logarithmic dependence of the bed height fluctuations on $(1.01 - e)$.

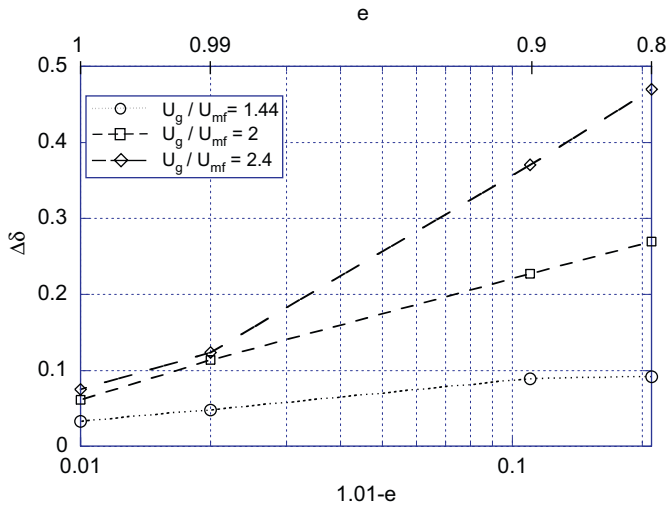

Fig. 12. Relative fluctuation vs. restitution coefficient—coarse powder, Princeton model.

These results agree with those of many other authors (Chandrasekaran, 2005; Chang and Louge, 1992; Goldschmidt et al., 2001; Hoomans et al., 1996; Lindborg et al., 2007; Lu et al., 2005; Pita and Sundaresan, 1991; Taghipour et al., 2005; Wang and Ge, 2006) on the fact that bed dynamics is quite sensitive to the restitution coefficient and that a decrease of its value leads to the formation of larger bubbles (i.e., larger fluctuations) (Goldschmidt et al., 2004). But this study seems to be the first one in which the influence of e is studied systematically for a wide range of processing parameters, highlighting different effects on bed expansion and fluctuations depending on the fluidization regime, which cannot be determined based on intuition.

From Figs. 8–10, it appears that the restitution coefficient value of 0.8 is more physically realistic than other values.

4.3.3. Influence of the internal angle of friction

For this study, 3-D calculations were done with value of e set to 0.8 but varying the value of the internal angle of friction ϕ. Regardless of the particle diameter and the solid stress model chosen, the effects of ϕ were the following:

- decreasing ϕ from 40° to 30° or 10°, bed expansions calculated did not change significantly (variations in $\overline{\delta}$ are less than ±10%),
- decreasing ϕ from 40° to 30°, the heights of fluctuation decreased by about 20% on an average over the bed cycles and over all the simulations and
- decreasing ϕ from 40° to 10°, the heights of fluctuation decreased by about 53% on an average over the bed cycles and over all the simulations.

Note that the decreases in the height of fluctuations were always concomitant with increases in fluctuation frequencies.

From these observations, we can conclude that the heights of fluctuation linearly increases with the internal angle of friction in the range of the operating conditions studied, whereas the bed expansion does not change. This means that a bed of irregular particles with a rough surface tends to be more fluctuating than a bed of spherical particles with a smooth surface. This could be explained by the fact that a higher value of ϕ implies more friction between the particles, which could promote the formation of larger heterogeneities in the granular flow. To the best of our knowledge, no other study in the literature has reported the above effect of ϕ.

Finally, it was observed that using free slip BC instead of J&J BC for solids did not change the trends observed for the influence of the restitution coefficient and the internal angle of friction.

5. Conclusion

This study has been performed to better understand the influence of closure models for the granular stresses and of their associated parameters on the simulation of gas–solid fluidized beds. The bed expansion and height of fluctuations were experimentally measured in a fluidized bed of alumina (Geldart's group B) particles of two mean diameters for different superficial gas velocities U_g. For the fine particles, the regime was always bubbling, whereas for the coarse particles both bubbling and slugging regimes appeared depending on U_g. Numerical simulations were performed using the MFIX code. A specific data processing protocol was developed to extract from the simulation results the values of the mean bed expansion ratio $\overline{\delta}$ and the relative height of fluctuations $\Delta\delta$. Numerous simulations were performed using 2-D and 3-D geometries, two different particle stress models (the Schaeffer and Princeton models) with different values of the restitution coefficient (e) and of the internal angle of friction (ϕ) and two kinds of wall boundary conditions for solids, free slip and Johnson and Jackson partial slip.

The results first show that 3-D simulations are necessary for correctly reproducing the experimental bed expansions and heights of fluctuation; the 2-D simulations widely overestimated both the quantities.

The simulations also demonstrate the great importance of the particle stress model for the simulation of bubbling and slugging fluidized bed. Predictions with the Princeton model agreed satisfactorily with experimental data for average and dynamic bed characteristics, although fluctuation frequencies were moderately overpredicted. The Schaeffer model calculated beds with larger heights of fluctuations as compared to the Princeton model.

The Princeton model was then used to study the influence of wall boundary conditions for solids on the predicted bed expansion. The difference in the bed expansion ratios predicted with free slip and Johnson and Jackson boundary conditions was very small, except for one data point (coarse powder at the highest velocity tested). So both the boundary conditions appear to be equally good for the simulation conditions investigated in this paper.

The effect of the restitution coefficient (e) seems to depend on the fluidization regime: in the bubbling regime, an increase in e leads to larger bed expansions and lower heights of fluctuations, whereas it leads to unchanged or lower bed expansions and to a massive reduction in the heights of fluctuations in the slugging regime.

The angle of internal friction (ϕ) has minimal influence on the bed expansion, but a reduction in ϕ leads to a significant reduction in the height of fluctuations.

Notation

c	drag constant for Eq. (10),dimensionless
d	drag constant for Eq. (10),dimensionless
d_p	particle mean diameter,m
$D_{s,ij}$	rate of strain tensor,solid phase,s^{-1}
e	restitution coefficient,dimensionless
e_w	particle–wall restitution coefficient,dimensionless
f_{gi}	fluid flow resistance due to porous media,N/m^3
g_i	acceleration due to gravity,m/s^2
g_0	radial distribution function at contact,dimensionless

H	expanded bed height,m
$\overline{H}$	mean expanded bed height,m
H_{max}	maximum expanded bed height,m
H_{mf}	expanded bed height at minimum fluidization,m
H_{min}	minimum expanded bed height,m
I_{2D}	second invariant of the deviator of the strain rate tensor for solid phase,s^{-2}
I_{gmi}	momentum transfer from fluid phase to solid phase,N/m^3
$I_{k'ki}$	momentum transfer from phase k' to phase k,N/m^3
J_m	collisional dissipation,m^2/s^3
P	pressure,Pa
P_c	critical pressure in solid phase given by Eq. (29),Pa
P_f	frictional pressure in solids phase,Pa
Re_m	solids phase particle Reynold number, dimensionless
S_{mij}	solids phase stress, Pa
$\mathbf{S}$	solids phase stress tensor, Pa
t	time, s
$\mathbf{u}$	velocity vector, m/s
u_{ki}	velocity of phase k, m/s
u_m	tangential velocity of solids, m/s
U_g	superficial gas velocity, m/s
U_{mf}	superficial gas velocity at minimum fluidization, m/s
V_{rm}	the ratio of the terminal velocity of a group of particles to that of an isolated particle, dimensionless
x	coordinate, m

Greek letters

α	a constant with value of 1.6, dimensionless
β_{gm}	coefficient for the interphase force between the fluid phase and the solids phase, kg/m^3 s
$\overline{\delta}$	mean bed expansion ratio, dimensionless
$\delta(H)$	ratio of bed expansion defined by Eq. (1), dimensionless
δ_{ij}	Kronecker symbol, dimensionless
$\Delta\delta$	relative mean height of fluctuations, dimensionless
ε	volume fraction, dimensionless
ε_g^*	critical void fraction, dimensionless
ε_0	void fraction at packing, dimensionless
ε_{mf}	void fraction at minimum fluidization conditions, dimensionless
$\varepsilon_{s\text{-}mf}$	solid fraction at minimum fluidization conditions, dimensionless
$\varepsilon_s^{\max}$	solid fraction at critical void fraction $(=1-\varepsilon_g^*)$,dimensionless
$\varepsilon_{sf}^{\min}$	solid volume fraction at maximum packing limit, dimensionless
η	function of restitution coefficient defined by Eq. (23), dimensionless
Θ	granular temperature, m^2/s^2
κ_m	solids conductivity of granular energy, W/m K
μ	viscosity, kg/m s
μ_f	solids frictional viscosity, kg/m s
Π_m	granular temperature exchange term, kg/ms^3
ρ	miscroscopic (material) density, kg/m^3
τ_{kij}	stress tensor of phase k, Pa
ϕ	internal angle of friction, deg
ϕ_p	specularity coefficient (chosen as 0.6), dimensionless

Subscripts and superscripts

g	gas
i,j	indices to identify vector and tensor components
k	phase k (fluid or solids)
m	solids phase

Acknowledgments

Simulations presented in this paper were carried out with the help of I. Touche from LGC, using (i) the Grid'5000 experimental test, an initiative from the French Ministry of Research through the ACI GRID incentive action, INRIA, CNRS and RENATER and other contributing partners (see https://www.grid5000.fr) and (ii) the French supercomputing centers CalMip and CINES. This project has been supported by the French ANR-Réseau National Matériaux et Procédés. Sreekanth Pannala and Madhava Syamlal acknowledge the support of US DOE's Fossil Energy program.

References

Agrawal, K., Loezos, P.N., Syamlal, M., Sundaresan, S., 2001. The role of meso-scale structures in rapid gas–solid flows. Journal of Fluid Mechanics 445, 151–185.

Barrett, R., Berry, M., Chan, T., Demmel, J., Donato, J., Dongarra, J., Eijkhout, V., Pozo, R., Romine, C., van der Vorst, H., 2006. Templates for the Solution of Linear Systems: Building Blocks for Iterative Methods. second ed. SIAM, Philadelphia, PA. Available at ⟨http://www.netlib.org/templates/templates.pdf⟩.

Benyahia, S., Syamlal, M., O'Brien, T.J., 2006. Summary of MFIX equations 2005-4 ⟨http://www.mfix.org/documentation/MfixEquations2005-4-1.pdf⟩.

Cadoret, L., Reuge, N., Pannala, S., Syamlal, M., Coufort, C., Caussat, B., 2007. Silicon CVD on submicronic powders in vibrated fluidized bed. Surface & Coatings Technology 201 (22–23), 8919–8923.

Chandrasekaran, B., 2005. Master Science Thesis, University of Calgary, Calgary, Alberta, Canada.

Chandrasekaran, B.K., van der Lee, L., Hulme, I., Kantzas, A., 2005. A simulation and experimental study of the hydrodynamics of a bubbling fluidized bed of linear low density polyethylene using bubble properties and pressure fluctuations. Macromolecular Materials and Engineering 290, 592–609.

Chang, H., Louge, M., 1992. Fluid dynamic similarity of circulating fluidized beds. Powder Technology 70, 259–270.

Davidson, J.F., Harrison, D., 1963. Fluidized Particles. Cambridge University Press, Cambridge, UK.

Deen, N.G., Van Sint Annaland, M., Kuipers, J.A.M., 2006. Detailed computational and experimental fluid dynamics of fluidized beds. Applied Mathematical Modelling 30 (11), 1459–1471.

Deen, N.G., Van Sint Annaland, M., Van der Hoef, M.A., Kuipers, J.A.M., 2007. Review of discrete particle modeling of fluidized beds. Chemical Engineering Science 62, 28–44.

Ding, Y.L., Forster, R.N., Seville, J.P.K., Parker, D.J., 2001. Scaling relationships for rotating drums. Chemical Engineering Science 56, 3737–3750.

Enwald, H., Peirano, E., Almstedt, A.E., 1996. Eulerian two-phase flow theory applied to fluidization. International Journal of Multiphase Flow 22 (1), 21–66.

Goldschmidt, M.J.V., Kuipers, J.A.M., van Swaaij, W.P., 2001. Hydrodynamic modelling of dense gas-fluidised beds using the kinetic theory of granular flow: effect of coefficient of restitution on bed dynamics. Chemical Engineering Science 56 (2), 571–578.

Goldschmidt, M.J.V., Beetstra, R., Kuipers, J.A.M., 2004. Hydrodynamic modelling of dense gas-fluidised beds: comparison and validation of 3D discrete particle and continuum models. Powder Technology 142 (1), 23–47.

Gorham, D.A., Kharaz, A.H., 2000. The measurement of particle rebound characteristics. Powder Technology 122, 193–202.

Guenther, C., O'Brien, T., Syamlal, M., 2001. A numerical model of silane pyrolysis in a gas–solids fluidized bed. In: Fourth International Conference on Multiphase Flows, vol. 1, New Orleans, LA.

Helland, E., Occelli, R., Tadrist, L., 2005. Numerical study of cluster and particle rebound effects in a circulating fluidised bed. Chemical Engineering Science 60, 27–40.

Hoomans, B.P.B., Kuipers, J.A.M., Briels, W.J., van Swaaij, W.P.M., 1996. Discrete particle simulation of bubble and slug formation in a two-dimensional gas-fluidised bed: a hard-sphere approach. Chemical Engineering Science 51 (1), 99–118.

Jackson, R., 1983. Some mathematical and physical aspects of continuum models for the motion of granular materials. In: Meyer, R.E. (Ed.), Theory of Dispersed Multiphase Flow. Academic Press, New York.

Johansson, K., van Wachem, B.G.M., Almstedt, A.E., 2006. Experimental validation of CFD models for fluidized beds: influence of particle stress models, gas phase compressibility and air inflow models. Chemical Engineering Science 61 (5), 1705–1717.
Johnson, P.C., Jackson, R., 1987. Frictional-collisional constitutive relations for granular materials with application to plane shearing. Journal of Fluid Mechanics 176, 67–93.
Lettieri, P., Di Felice, R., Pacciani, R., Owoyemi, O., 2006. CFD modelling of liquid fluidized beds in slugging model. Powder Technology 167 (2), 94–103.
Limtrakul, S., Rotjanavijit, W., Vatanatham, T., 2007. Lagrangian modeling and simulation of effect of vibration on cohesive particle movement in a fluidized bed. Chemical Engineering Science 62 (1–2), 232–245.
Lindborg, H., Lysberg, M., Jakobsen, H.A., 2007. Practical validation of the two-fluid model applied to dense gas–solid flows in fluidized beds. Chemical Engineering Science 62, 5854–5869.
Lu, H., Wang, S., Zhao, Y., Li, Y., Gidaspow, D., Ding, J., 2005. Prediction of particle motion in a two-dimensional bubbling fluidized bed using discrete hard-sphere model. Chemical Engineering Science 60, 3217–3231.
Lun, C.K.K., Savage, S.B., Jeffrey, D.J., Chepurniy, N., 1984. Kinetic theories for granular flow: inelastic particles in Couette flow and slightly inelastic particles in a general flow field. Journal of Fluid Mechanics 140, 223–256.
Makkawi, Y.T., Wright, P.C., Ocone, R., 2006. The effect of friction and inter-particle cohesive forces on the hydrodynamics of gas–solid flow: a comparative analysis of theoretical predictions and experiments. Powder Technology 163 (1–2), 69–79.
Massoudi, M., 1986. Application of mixture theory to fluidized beds. Ph.D. Thesis, University of Pittsburgh, Pittsburgh, PA.
Patankar, S.V., 1980. Numerical Heat Transfer and Fluid Flow. Hemisphere Series on Computational Methods in Mechanics and Thermal Science. Hemisphere Publishing Corporation, Washington, DC.
Patil, D.J., van Sint Annaland, M., Kuipers, J.A.M., 2005. Critical comparison of hydrodynamic models for gas–solid fluidized beds—Part I: bubbling gas–solid fluidized beds operated with a jet. Chemical Engineering Science 60 (1), 57–72.
Pita, J.A., Sundaresan, S., 1991. Gas–solid flow in vertical tubes. A.I.Ch.E. Journal 37 (7), 1009–1018.
Savage, S.B., 1998. Analyses of slow high-concentration flows of granular materials. Journal of Fluid Mechanics 377, 1–26.
Schaeffer, D.G., 1987. Instability in the evolution equations describing incompressible granular flow. Journal of Differential Equations 66, 61–74.
Srivastava, A., Sundaresan, S., 2003. Analysis of a frictional–kinetic model for gas–particle flow. Powder Technology 129 (1–3), 72–85.
Syamlal, M., 1998. MFIX documentation: numerical technique. Technical Report DOE/MC31346-5824 (DE98002029), Morgantown Energy Technology Centre, Morgantown, West Virginia (can be downloaded from ⟨http://www.mfix.org⟩).
Syamlal, M., O'Brien, T.J., 2003. Fluid dynamic simulation of O_3 decomposition in a bubbling fluidized bed. A.I.Ch.E. Journal 49, 2793–2801.
Syamlal, M., Rogers, W., O'Brien, T.J., 1993. MFIX documentation: theory guide. Technical Report DOE/METC-94/1004 (DE9400087), Morgantown Energy Technology Centre, Morgantown, West Virginia (can be downloaded from Multiphase Flow with Interphase eXchanges (MFIX) website: ⟨http://www.mfix.org⟩).
Taghipour, F., Ellis, N., Wong, C., 2005. Experimental and computational study of gas–solid fluidized bed hydrodynamics. Chemical Engineering Science 60 (24), 6857–6867.
Tatemoto, Y., Mawatari, Y., Noda, K., 2005. Numerical simulation of cohesive particle motion in vibrated fluidized bed. Chemical Engineering Science 60, 5010–5021.
Terzaghi, K., 1942. Theoretical Soil Mechanics. Wiley, New York, NY.
Tuzun, U., Houlsby, G.T., Nedderman, R.M., Savage, S.B., 1982. The flow of granular materials—II, velocity distributions in slow flow. Chemical Engineering Science 37, 1691–1789.
Van Wachem, B., Schouten, J.C., van den Bleek, C.M., Krishna, R., Sinclair, J.L., 2001. Comparative analysis of CFD models of dense gas–solid systems. A.I.Ch.E. Journal 47 (5), 1035–1051.
Wang, J., Ge, W., 2006. Multi-scale analysis on particle-phase stresses of coarse particles in bubbling fluidized beds. Chemical Engineering Science 61, 2736–2741.
Weber, M.W., Hrenya, C.M., 2006. Square-well model for cohesion in fluidized beds. Chemical Engineering Science 61 (14), 4511–4527.
Xie, N., Battaglia, F., Pannala, S., 2008a. Effects of using two-versus three-dimensional computational modeling of fluidized beds: part I, hydrodynamics. Powder Technology 182 (1), 1–13.
Xie, N., Battaglia, F., Pannala, S., 2008b. Effects of using two-versus three-dimensional computational modeling of fluidized beds: part II, budget analysis. Powder Technology 182 (1), 14–24.
Xu, B.H., Zhou, Y.C., Yu, A.B., Zulli, P., 2002. Force structures in gas fluidized beds of fine powders. In: Proceedings of the World Congress on Particle Technology vol. 4, Sydney, Australia.